Diffraction of Inelastically Scattered Electrons in Tungsten at Low Energies

J. O. Porteus
Michelson Laboratory, China Lake, California 93555

ABSTRACT

A study on a clean tungsten (110) surface of the angular and energy dependence of electron scattering by plasmons near 100 eV shows well defined diffracted beams of inelastic electrons. The positions of these beams relative to diffracted elastic beams suggests that plasmon scattering and diffraction are not independent. Intensity vs. voltage maxima for the inelastic beams agree in most cases with those for corresponding elastic beams, although some differences are apparent. Possible application of results include studies of electron-plasmon interaction phenomena and additional information on LEED interpretations.

INTRODUCTION

The study of electron scattering by plasmons at low energies ordinarily requires diffraction or an intervening scattering event to return the electrons from the sample for observation. In addition to information on inelastic interactions, such multiple processes may also provide a useful adjunct to elastic scattering in studies of the diffraction process itself. Previous work[1-4] on the distribution of low energy electrons inelastically scattered from single-crystal surfaces indicates that diffraction plays a

significant role. These measurements were generally limited to the immediate neighborhood of a few elastic diffraction maxima, where intense inelastic scattering with a relatively wide distribution of energy is commonly observed. In the present work, measurements are extended to regions of the diffraction pattern remote from elastic maxima, where the plasmon loss maxima are found to be more distinct. In addition to a broader scope, a clearer view of the diffraction phenomena is obtained. Tungsten (110) was chosen as the surface for investigation because it has been extensively studied, can be easily cleaned, and because a recent study of the total scattering[3] identifies two pronounced loss maxima from a surface and a volume plasmon loss. A relevant optical study on this surface has also been reported.[5]

EXPERIMENTAL METHOD

1. Apparatus

A schematic view of the diffractometer is given in Fig. 1. Electrons thermionically emitted at the tungsten filament 1 are extracted from the space charge region by the electrode 3, focused by the Wehnelt cylinder 2, and decelerated at the anode 4. Two pairs of vertical deflectors, 6 and 7, permit accurate positioning of the beam in the horizontal plane of rotation of the collector 9, or slightly out of this plane to correct for minor sample misalignment. The vertical deflection obscures the filament from the sample and also provides some monochromatization, giving a resulting beam energy-width of about 0.5 eV. An additional pair of deflectors 5 permit horizontal aiming. After traversing a coarse limiting slit the beam strikes the sample surface 8, which ideally contains the collector rotation

axis. Fine collimation is provided by a pair of circular collector apertures 10, which select a 1.3° cone of electrons emerging from a limited area of the sample. The effective incident beam divergence is thereby restricted to about 0.5°, depending somewhat on the collector position. A high-resolution retarding lens immediately preceding the Faraday cylinder excludes electrons with energies less than a preselected value. The collected electron signal is amplified by a Cary model 36 vibrating-reed amplifier and, after filtering, is displayed on an XY recorder as a function of either retarding, or primary beam voltage. A synchronized programming of anode and vertical deflection voltages with collector motion provides automatic recording of intensity vs. voltage data. The sample azimuth can either be set or varied continuously for rapid diffraction pattern scanning at normal incidence by rotating the sample about its normal, using the rotating drive 15 coupled through the manipulating rod 14. With the rod disengaged by means of the sliding drive 16, the sample can be rotated about the vertical axis to select the desired angle of incidence. For direct observation of the incident beam, or for sample cleaning, the sample may be withdrawn to the position 11. Electron-bombardment heating on the reverse side of the sample wafer is provided by the gun 13, while a gas stream can be directed onto the front surface through the nozzle 12. All drives are magnetically coupled through the vacuum envelope with well concentrated fields, permitting angular settings accurate to 0.2°. All drive magnets are either field-compensated or can be operated intermittently to eliminate magnetic field distortions. All parts except the electromagnets are of nonferromagnetic materials, principally stainless steel. A freon-cooled Orb-Ion pump and baffle provide a field-free working vacuum in the

low 10^{-10} torr range after system bakeout. With the aid of Helmholtz coils the residual magnetic field in the diffraction region is maintained at less than 20 milligauss.

2. Sample

The sample is a 3/8" diameter by .020" thick wafer, which has been spark-cut from 110 oriented, single floating-zone refined, tungsten single crystal obtained from Aremco. The surface for study was mechanically ground to within 0.05 degrees of the (110) planes with the aid of a Siemens x-ray diffractometer and a specially constructed jig. This was followed by mechanical polishing and electropolishing to a mirror finish. Final cleaning was performed in ultrahigh vacuum by intense heating, followed by oxidation and desorption in the usual manner[2,3] until the clean tungsten diffraction pattern was observed. As an additional check on cleanliness the secondary electron spectrum was examined for Auger peaks from possible contaminants,[3] and none were detected. However, the sensitivity was considerably limited by the small collector acceptance angle.

DISCUSSION AND RESULTS

1. Elementary models

A model first proposed by Davisson and Germer[6] for inelastic scattering accompanied by diffraction is illustrated for the case of normal incidence in Fig. 2. The incident beam $\underset{\sim}{K}$ is first diffracted into $\underset{\sim}{K}'$ and is then scattered into a cone of inelastic loss beams such as $\underset{\sim}{K}''$ surrounding the diffracted elastic beam. Since the primary beam energy governs the diffraction in this model, this type of double process will be designated as I. Note that the loss beam maxima coincide with those of the diffracted elastic beam, i.e. when $\underset{\sim}{K}'$ terminates on a reciprocal lattice point P.

A second type of model, which was first proposed by Turnbull and Farnsworth,[4] is shown for normal incidence in Fig. 3. Here the incident beam $\underset{\sim}{K}$ is first inelastically scattered into a cone about the forward direction. Certain component beams in this inelastic cone, such as $\underset{\sim}{K}_1'$ and $\underset{\sim}{K}_2'$, are then selectively diffracted into respective beams such as $\underset{\sim}{K}_1''$ and $\underset{\sim}{K}_2''$, which form a corresponding emergent cone (not shown). Since diffraction is governed by the energy of the inelastic beams (secondary energy), this type of double process will be designated as II. Because of the difference in length of primary and secondary wave vectors the emergent loss beams do not generally approximate the direction of the diffracted elastic beam unless the energy loss is small. However, they do coincide with the position the elastic beam would have at the corresponding primary energy and angle of incidence. If the forward scattering cone is strongly concentrated about $\underset{\sim}{K}_1'$ one might expect diffraction by the reciprocal lattice rod, as illustrated by $\underset{\sim}{K}_1''$, in analogy with elastic diffraction. However, if the cone is broad one might expect a type of diffraction more closely resembling Kikuchi line phenomena. The beam $\underset{\sim}{K}_2'$, for example, which satisfies the condition for Bragg reflection, can give rise to the component $\underset{\sim}{K}_2''$ of a Kikuchi excess line associated with the inelastic scattering.

Although both models can easily include dynamical effects in the diffraction stage of the double process, the assumed independence of the diffraction and inelastic scattering is basically a kinematic concept. In spite of this artifical aspect, the models offer a convenient basis for discussion of present results.

An important difference between I and II lies in the fact that in II the diffraction is dispersive in the inelastic scattering whereas in I it

is not. Thus features of the inelastic scattering corresponding to different energy losses, which appear at essentially the same diffraction positions in I, may appear in quite different positions in II. The dispersion associated with the inelastic scattering event must, of course, be present in both I and II, but this may be comparatively small. Also, II requires coherence of the inelastically scattered electrons so that a smaller incoherent background would be expected to accompany II.

2. Observations

When the collector is near an elastic beam, retarding-field scans of the electron energy distribution generally show, in agreement with previous observers, a strong inelastic background scattering which increases with decreasing energy loss. Some evidence of discrete-loss scattering was observed but these features are usually broad and largely obscured by the background. An increase of background intensity with increasing elastic intensity as predicted by I was also observed. However, in some situations a dispersive redistribution of background energy with varying collector angle was seen, indicating II. In addition to this mixture of double processes near the elastic beam, two experimental complications were generally associated with the large elastic component. One of these was a slight reduction in collector resolution, probably due to space charge distortion of the retarding field by the relatively large accumulation of retarded electrons. A more serious problem of apparently similar origin was an instability in the collected current, which made inelastic measurements difficult within 2° of the elastic beam.

Figure 4 shows the results of a sequence of retarding-field scans made at a fixed collector position in the 01 azimuth and away from the 02 elastic

beam. Each of the heavy solid curves represents an electron energy distribution, where a localized rise in collector current corresponds to a peak in the energy spectrum. The sharp rise at zero loss results from elastic and thermal scattering, while the more gradual rise which shifts (dashed line) as the primary energy is changed is associated with inelastic scattering. If one compares the relative heights of the inelastic rise with the aid of the tangent lines, a maximum is observed at a primary energy of about 54 eV and a corresponding energy loss of 10.5 eV measured from the midpoint of the elastic rise. Scans at higher primary energies with the same collector setting reveal an additional loss maximum at an energy loss of 22 eV. These values are somewhat lower than the 12.5 and 23.5 eV energy loss values reported for surface and volume loss maxima, respectively, in the total scattering.[3] The different average plasmon dispersion resulting from the larger angular distribution in the total scattering measurements could account for these differences.[7] The optical data on tungsten[5] is questionable regarding sample contamination and, furthermore, shows a large unexplained discrepancy with electron loss measurements concerning the volume loss. For these reasons the interpretation of the losses given in the total scattering study[3] is adopted here.

The observed shift of the inelastic rise in Fig. 4 over the 8 eV range of primary energies shown amounts to 6.5 eV, as compared to an 8 eV maximum shift from diffractive dispersion predicted by model II under the following conditions: (1) infinitely narrow scattering cone, and (2) infinite angular resolution, including zero collector acceptance angle and zero thickness of the reciprocal lattice rod. Departure from these ideal conditions could

easily explain the smaller observed shift. The dispersion contribution from scattering by the surface plasmon, which should contribute to the curvature of the dashed line of Fig. 4, is evidently too small to be detected here.

A search for loss maxima was made in two azimuths of the diffraction pattern at normal incidence. Either the primary energy or the collector position was held fixed and the other varied for each scan sequence. Results for the 11 azimuth are summarized in Fig. 5, where observed maxima are compared in terms of colatitude angle and secondary energy, i.e. primary energy minus energy loss. Surface and volume loss maxima largely coincide on this plot in agreement with model II and, except for some isolated maxima, form two inelastic 11 beams running parallel to the 11 elastic beam. However, the inelastic beams show a definite shift to higher energy and/or angle relative to the normally incident elastic beam, which is in disagreement with II if the scattering is symmetrical in the forward direction. Although the overall scattering contributing to all inelastic beams must show this symmetry at normal incidence, an asymmetric scattering, if compensated, can be associated with a particular beam. This, however, implies coupling between the two elements of the double process. Coupling between diffraction and inelastic scattering is regarded as the most plausible explanation of the shift. An explanation on the basis of different effective inner potentials for the diffraction of elastic vs. inelastic electrons can be ruled out, as will be shown.

Little evidence is found of beams associated with inelastic Kikuchi lines, which might be expected with a wide scattering cone. In terms of Fig. 5 these beams should lie along the paths followed by elastic beam

maxima as the angle of incidence is varied. Such a path with a possibly associated beam is indicated by the dashed line in the figure. Figure 6 shows loss beam positions observed in the 01 azimuth relative to the 02 elastic beam. The results are essentially the same as for the 11 azimuth with even less evidence for inelastic Kikuchi beams.

Measurement of the inelastic scattering cone angle in the plane of a given azimuth is complicated by the dispersion and by diffracted intensity variations along the reciprocal lattice rod. However, the scattering cone angle normal to the azimuth plane should be directly related to the corresponding cone angle of the observed loss beams. Accordingly, retarding field scan sequences of the 11 and the 02 loss beams were made across their respective azimuths, and the angles subtended by their half-maximum intensity cones were determined without correction for instrumental broadening effects. The 11 loss beams measured at 80 and 70 eV primary energies, respectively, both gave a value of roughly 6°, while the corresponding 02 beams measured at 65 and 55 eV, respectively, gave a value of roughly 8°. No significant differences were noted between the surface and volume loss angular distributions. A theoretical calculation of the scattering angular dependence appropriate to the present experimental conditions is in progress,[8] but values are not yet available for comparison.

By simultaneously varying the primary energy and collector position, it is possible to track a loss beam in a sequence of retarding-field scans. The varying intensity of the loss beam in this sequence provides an intensity vs. voltage curve for this beam. Figure 7 compares the observed peaks in such curves for the 11 surface and volume loss beams with the 11 elastic curve. When compared in terms of secondary energy the agreement of peak positions

is good--too good in fact to permit explanation of the anomalous shift in loss beam positions as an inner-potential effect. Figure 8 shows similar results for the 02 beams, again with generally good agreement of peak positions. Although a few possibly important differences are apparent, the essential similarity of the elastic and inelastic data is in support of II, at least as a first approximation.

The similarities apparent in Figs. 7 and 8 suggest that plasmon scattering studies may have an important bearing on the interpretation of elastic intensity vs. voltage data. This would not be the case if the scattering were predominantly by image forces before penetration, as Heidenreich has proposed for fast electrons,[9] since elastic and inelastic intensity vs. voltage data would then contain basically the same information regarding diffraction. However, the present evidence for coupling between inelastic scattering and diffraction and minor differences which appear in the last two figures do not favor this interpretation. More definitive experiments with varying surface conditions are needed to explore this interesting possibility.

SUMMARY

The double process of electron scattering by plasmons and subsequent diffraction has been investigated at low energies on a tungsten (110) surface. Two well-defined inelastic beams corresponding to previously observed plasmon losses, and showing diffractive dispersion, were found to accompany an elastic beam. The position of the loss beams indicate that an adequate theory of scattering by plasmons must include coupling of the scattering with diffraction. Intensity vs. voltage characteristics of the loss beams

were studied and were found to be similar to those of the associated elastic beam when plotted as a function of secondary energy. This is expected on the basis of the double process with dynamical diffraction. Possible application of the present results include studies of electron-plasmon interaction at low energies and additional information on LEED interpretations.

ACKNOWLEDGMENTS

Grateful acknowledgments are due to Dr. E. Bauer for many helpful discussions and for reviewing the manuscript; also to Dennis K. Burge for calling author's attention to the optical data. This work was supported in part by the National Aeronautics and Space Administration under Contract No. R-05-030-001.

REFERENCES

1. Paul P. Reichertz and H. E. Farnsworth, Phys. Rev. 75, 1902 (1949).
2. R. M. Stern, Appl. Phys. Letters 5, 218 (1964).
3. L. N. Tharp and E. J. Scheibner, J. Appl. Phys. 38, 3320 (1967).
4. John C. Turnbull and H. E. Farnsworth, Phys. Rev. 54, 509 (1938).
5. D. W. Juenker, L. J. LeBlanc and C. R. Martin, J. Opt. Soc. Am. 58, 164 (1968).
6. C. Davisson and L. H. Germer, Phys. Rev. 30, 705 (1927).
7. H. Raether, in Springer Tracts in Modern Physics (Springer-Verlag, Berlin, 1965), Vol. 38, p. 140.
8. E. Bauer, private communication.
9. R. D. Heidenreich, J. Appl. Phys. 34, 964 (1963).

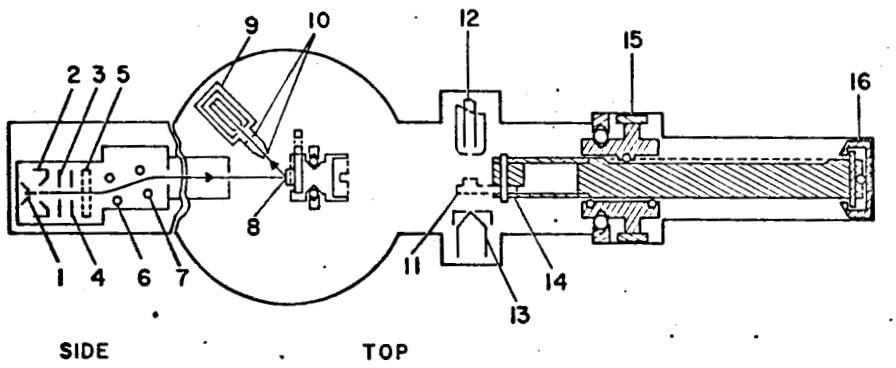

Fig. 1. Schematic of the diffractometer. The electron gun is shown rotated 90° relative to the rest of the apparatus.

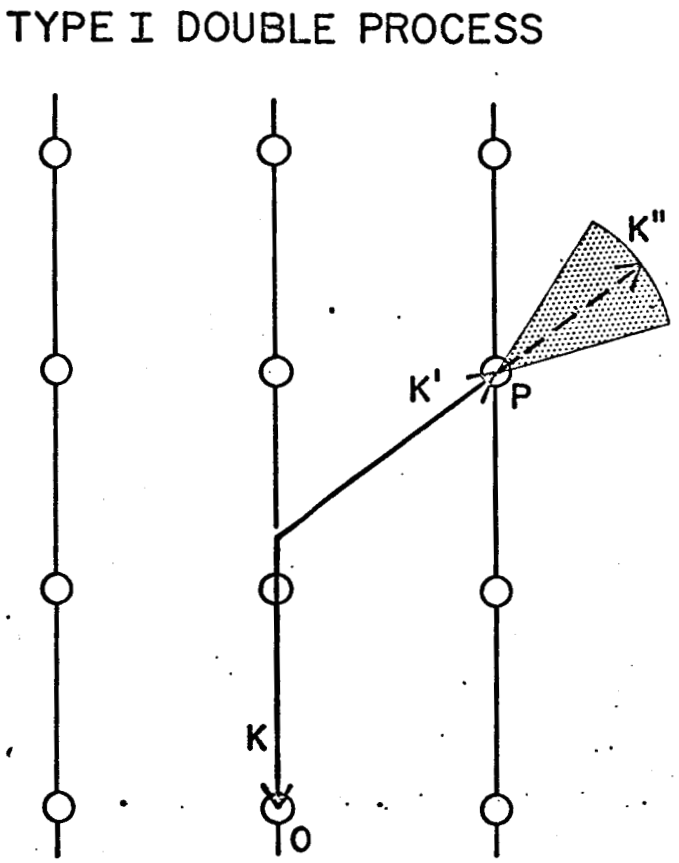

Fig. 2. The model of Davisson and Germer for combined diffraction and inelastic scattering.

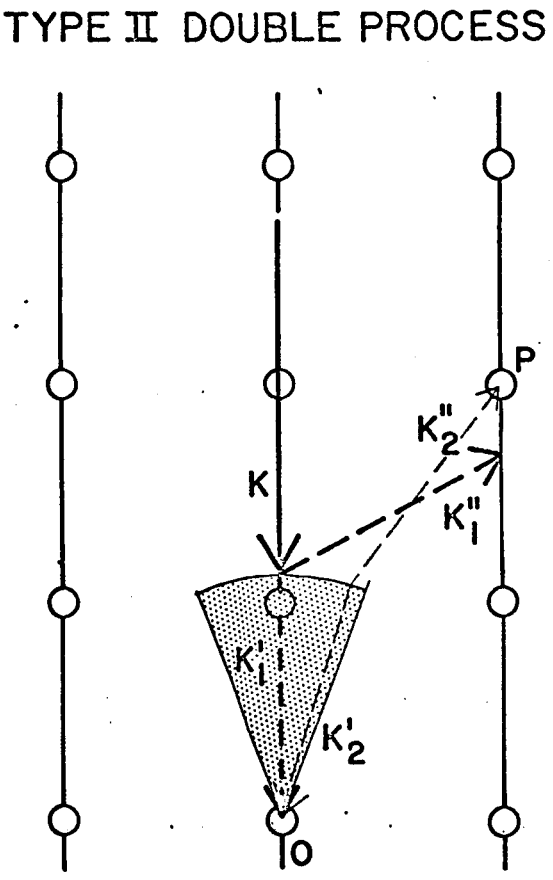

Fig. 3. The model of Turnbull and Farnsworth for combined diffraction and inelastic scattering.

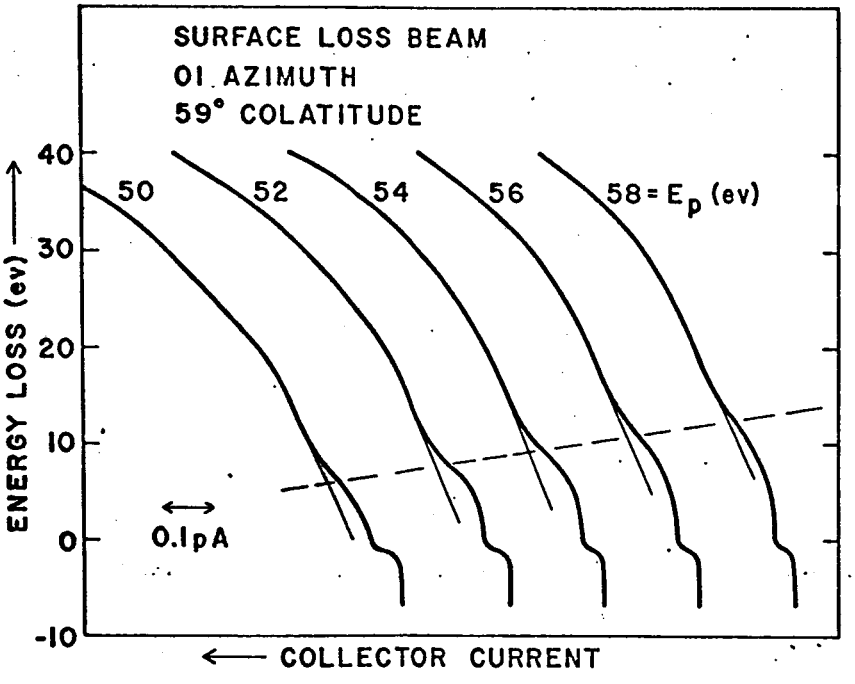

Fig. 4. Retarding-field scan sequence through a surface loss beam.

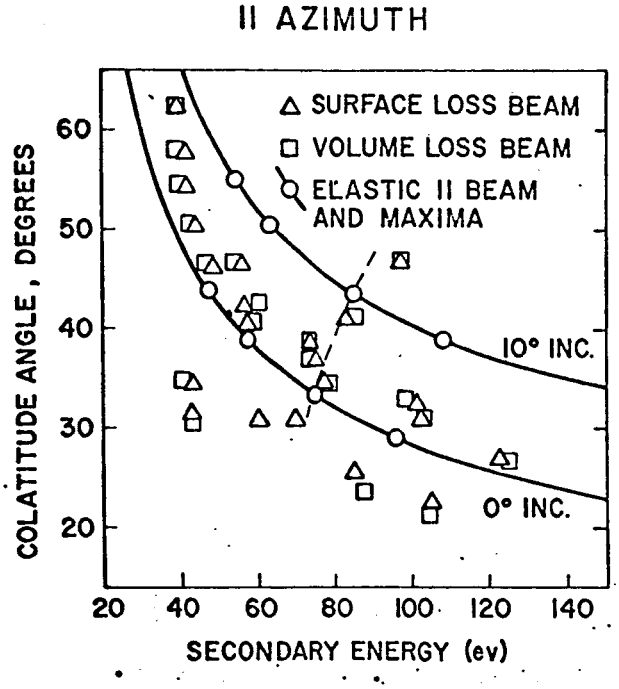

Fig. 5. Distribution in secondary energy and colatitude angle of loss beams at normal incidence in the 11 azimuth. The 11 elastic beam at normal and 10° incidence is shown for comparison.

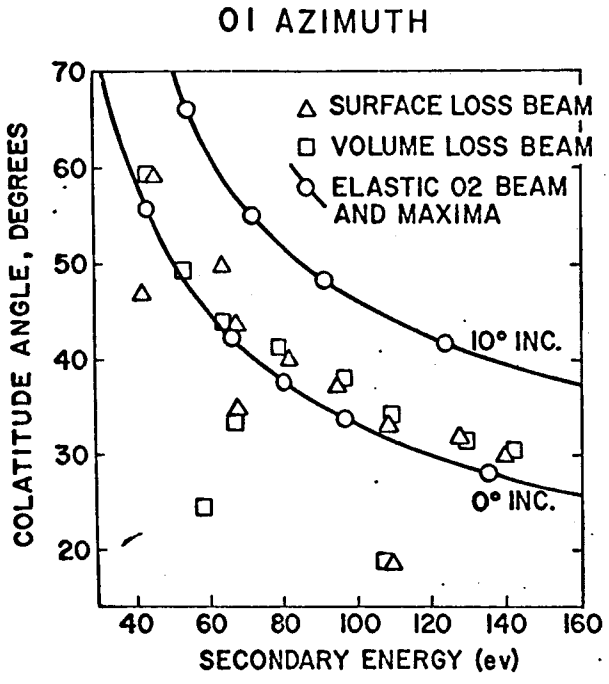

Fig. 6. Distribution in secondary energy and colatitude angle of loss beams at normal incidence in the 01 azimuth. The 11 elastic beam at normal and 10° incidence is shown for comparison.

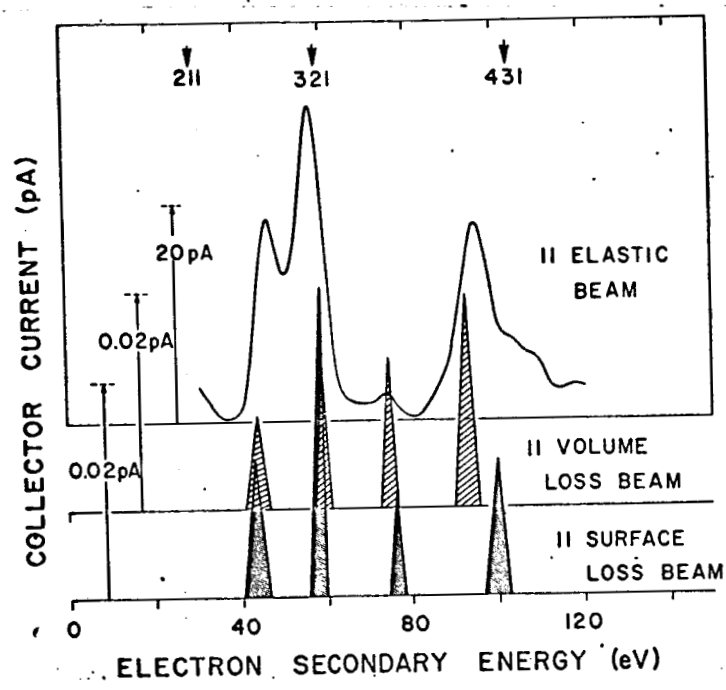

Fig. 7. Intensity vs. voltage features of ll elastic and loss beams compared in terms of secondary energy. The heights of the triangles indicate maximum collector signal at peaks in the loss beams. Bases of the triangles indicate uncertainty in peak positions. All measurements were made at normal incidence.

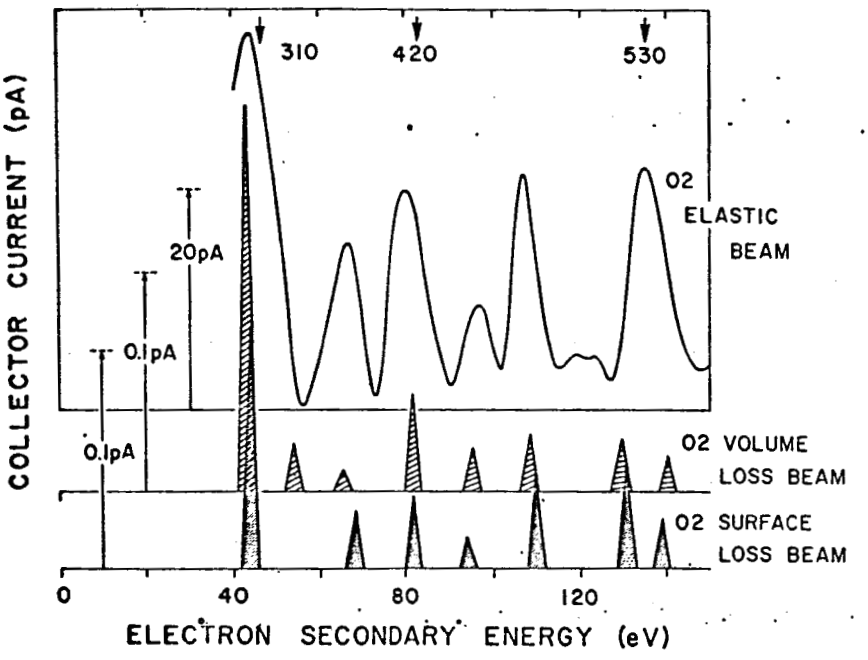

Fig. 8. Intensity vs. voltage features of 02 elastic and loss beams compared in terms of secondary energy. Triangles have the same significance as in Fig. 7. All measurements were made at normal incidence.